

STRANGENESS AND STATISTICAL HADRONIZATION: HOW TO STUDY QUARK–GLUON PLASMA*

JAN RAFELSKI

Department of Physics, University of Arizona
Tucson, AZ85721, USA

AND JEAN LETESSIER

Laboratoire de Physique Théorique et Hautes Energies
Université Paris 7, 2 place Jussieu, F-75251 Cedex 05, France

(Received September 3, 2003)

Statistical hadronization is presented as mechanism for (strange) particle production from a deconfined quark–gluon plasma (QGP) fireball. We first consider hadronic resonance production at RHIC as a test of the model. We present in detail how the hadrochemistry determines particle multiplicities and in case of sudden hadronization allows investigation of QGP properties. A comparative study of strange hadron production at SPS and RHIC is presented. The energy dependence of physical observables shows regularities and a potential discontinuity in the low RHIC range, when comparing these different energy domains. Considering the energy scan program at CERN-SPS we show that the K^+/π^+ discontinuity is a baryon density effect.

PACS numbers: 12.38.Mh, 24.10.Pa, 25.75.-q

1. Introduction

1.1. Setting the stage

It is believed today that a new state of matter has been formed in relativistic nuclear collisions at BNL–RHIC and at CERN–SPS, and perhaps even in 1800 GeV $p\bar{p}$ elementary interactions. The question of considerable interest is if this is the hot quark matter (quark–gluon plasma, QGP) state.

* Presented at the XLIII Cracow School of Theoretical Physics, Zakopane, Poland, May 30–June 8, 2003.

The paradigm of QGP originates in the quantum many body theory of quark matter [1, 2], which lead on to the formal recognition within the framework of asymptotically free quantum-chromodynamics (QCD) that, at a very high temperature, perturbative quark matter state must exist [3].

Further reasoning based on a study of the ‘boiling state’ of dense hadron gas within the scheme of Hagedorn’s statistical bootstrap of hadronic matter has lead from a different direction to the consideration of the transition to a hadron substructure phase [4, 5]. The present day lattice-QCD numerical simulations allows to evaluate more rigorously the expected properties of a equilibrium state of QGP, as we today call hot quark matter [6–9]. QGP is the equilibrium state of matter at high temperature and/or density. The question is if, in the short time such conditions are available in laboratory experiments, this new state of matter can be created. There is no valid first principles answer available today and we must address this issue experimentally.

It is obviously very hard to probe experimentally the QGP phase which exists a very short time. It is not widely accepted how a reaction involving formation of the deconfined state can be distinguished decisively from one involving reactions between individual confined hadrons. We observe in the final state of a high energy interaction reaction, irrespective if, or not, deconfinement has been achieved, a very large number of hadronic particles.

The phenomenon of J/Ψ and jet quenching probes the early stage of the deconfined phase. Its relation to deconfinement has been argued away in terms of effects of matter density and changes in primary production reaction mechanisms. Plasma photon radiation is buried in the background of final state photons from, *e.g.*, $\pi^0 \rightarrow \gamma\gamma$. Dileptons (that is in fact virtual photons) suffer from large experimental uncertainties, and a final state background which depends of new physics as well (hadron properties at finite temperature and density).

Perhaps the most promising path to a convincing evidence for the formation of the deconfined state in relativistic heavy ion collisions is the precision study of the production of soft hadrons. Insights into the nature of the hot hadronic matter fireball are gained from interpretation of an array of particle yields and spectra. A precise model description allows to evaluate the global properties such as energy, entropy, strangeness content of all particles produced. This opens up to further investigation the properties of the matter state that has hadronized.

Supporting this approach is the study of several reaction systems, *e.g.*, comparison of AA with NN and/or NA reactions. In this case, the change of particle yield when this contradicts the hadron rescattering model expectations is evidence of new physics. Normally one encounters in an AA experiment enhancement of expected yield comparing to NN reactions. More

recently, some have argued that the AA yield of (strange) hadrons is ‘normal’ and that the effect is due to a ‘suppressed’ NN base yield. This argument does not change the fact that in any case the AA yield does not arise from a sequence of NN reactions.

1.2. Survey of this work

The model we employ arises from the observation that hadron production is well described in a very large range of yields solely by evaluating the phase space size. Originally proposed by Fermi in order to describe multiparticle production in high energy cosmic ray interactions [10,11], in the past 40 year the Fermi model (*i.e.*, statistical hadronization) has been tried successfully in many particle production environments, beginning with p - p collisions at various energies, and branching out to heavy ion as well as the elementary non-hadronic e^+e^- reactions.

We begin, in Section 2, with a discussion of the role hadronic resonances play in testing the principles of statistical hadronization. We survey, in Subsection 2.1, the latest experimental hadronic resonance production results from RHIC. We next describe how particle yields and ratios can be obtained. We introduce, in Subsection 2.2, the ideas of hadrochemistry and show, in Subsection 2.3, how particle ratios determine hadronization parameters. We turn to the study of phase space densities in Subsection 2.4. We show that the entropy rich QGP phase hadronizes into chemical non-equilibrium pion gas that can absorb the entropy excess. For a more detailed discussion we refer to our earlier reviews [12–14].

We introduce strangeness as signature of deconfined QGP phase in Section 3. We discuss the interest in strangeness both from experimental and theoretical perspective in Subsection 3.1. We introduce, in Subsection 3.2, the two step strange hadron production process, in which the hadronization benefits from ample supply of strangeness already produced. This is the origin of multi strange hadron enhancement. We show, in Subsection 3.3, that the observed enhancement effect is genuine. In Subsection 3.4, we discuss how the outward collective flow of matter influences the resulting fireball hadronization conditions and assists the sudden hadronization.

Section 4 presents our findings about the hadronization at SPS and at RHIC. We define first the method of analysis in Subsection 4.1 and follow this through with a discussion of RHIC fits in Subsection 4.2. We then address the energy dependence of the statistical parameters characterizing the fireball source in Subsection 4.3. An interesting result that follows is about the behavior of energy per baryon stopping. Our primary interest is the strangeness yield which we address in Subsection 4.4.

Our study leads directly to the final question, is there a energy threshold for the onset of quark–gluon plasma formation, which we address in Section 5. An important element of our study is to identify observables which are independent of the different baryon densities reached. We look from this perspective at the kaon to pion ratio discontinuity reported at low end of SPS energy range. We show that this is a result of baryon density effect in Subsection 5.1. In Subsection 5.2 we discuss a mechanism of kaon to pion ratio enhancement arising from fast transverse expansion, and present the maximum enhancement expected at LHC. A brief evaluation of our findings and their importance follows in Subsection 5.3.

2. Statistical hadronization

2.1. Hadron resonances

The initial test of statistical hadronization approach to particle production is that within a particle ‘family’, particle yields with same valance quark content are in relation to each other thermally equilibrated. Thus the relative yield of, *e.g.*, $K^*(\bar{s}q)$ and $K(\bar{s}q)$ is controlled only by the particle masses m_i , statistical weights (degeneracy) g_i and the hadronization temperature T . In the Boltzmann limit one has (star denotes the resonance):

$$\frac{N^*}{N} = \frac{g^* m^{*2} K_2(m^*/T)}{g m^2 K_2(m/T)}. \quad (1)$$

Validity of this relation implies insensitivity of the quantum matrix element governing the coalescence-fragmentation production of particles to intrinsic structure (parity, spin, isospin), and particle mass. The measurement of the relative yield of hadron resonances is a sensitive test of the statistical hadronization hypothesis.

The experimental ratio [15–17]

$$\frac{(K^* + \overline{K^*})}{2K^-} = 0.26 \pm 0.03 \pm 0.07, \quad \frac{(K^* + \overline{K^*})}{2K^-} = 0.20 \pm 0.01 \pm 0.03,$$

has been measured, left for most central collisions with $\sqrt{s_{NN}} = 130$ GeV, and right for most central 200 GeV reactions, in RHIC-130, and RHIC-200 runs respectively (65 + 65 GeV and 100 + 100 GeV per nucleon head on collisions of two nuclear beams). The RHIC result naturally arises from the ratio Eq. (1) allowing for resonance decays within the statistical hadronization model for the temperature $T \simeq 145$ MeV. This is the favored solution of a fit which allows for chemical non-equilibrium [18], see Subsection 4.2.

However, the yield:

$$\frac{A(1520)}{A} = 0.022 \pm 0.01,$$

recorded in the RHIC-130 and RHIC-200 runs [19, 20], is two times smaller compared to statistical hadronization expectation. Statistical hadronization at higher temperature than $T = 145$ MeV does not resolve this discrepancy, but adds to it a K^*/K^- suppression.

These two ratios, seen together, are, at first, difficult to understand. Let us first note that an apparent production suppression may actually be detectability suppression. Namely, should the decay products of resonances rescatter on other particles after formation, their energies and momenta will change. Hence, not all produced resonances can be, in general, reconstructed from the decay products energies E_i and momenta p_i by testing for the invariant mass:

$$m^{*2} = (E_1 + E_2)^2 - (\vec{p}_1 + \vec{p}_2)^2. \quad (2)$$

The rescattering effect depletes more strongly the yields of shorter lived states. These decay sooner and are thus more within the dense matter system. If resonance yield is as predicted by statistical hadronization, the decay life span is expected to be larger than the hadronization time, *e.g.*,

$$c\tau_{K^*} = \frac{\hbar c}{\Gamma_{K^*}} = 3.9 \text{ fm} > c\tau_{\text{had}}.$$

This assures that most K^* decay after thermal freeze-out of decay products (K, π) in free space. On the other hand, we recall that the lifespan of $\Lambda(1520)$ is about 2.3 times longer than that of K^* . This means that contrary to the expectation derived from rescattering effect, it is the longer lived $\Lambda(1520)$ state for which we find the signature to be significantly depleted as compared to what could be maximally seen given the statistical hadronization yield.

A natural explanation of the $\Lambda(1520)$ signature suppression is in matter modification of the free space $\Gamma = 15.6 \pm 1$ MeV decay width [21]. This width corresponds to $c\tau = 12.6$ fm. Thus for sudden hadronization, implied by the observed yield of K^* , $\Lambda(1520)$ decay should occur well outside the reaction domain. However, if in medium width is at the level of 200 MeV, within a hadronization lifespan of 0.7 fm/c half of the produced $\Lambda(1520)$ yield would become unobservable due to rescattering of decay products. Such a resonance width of 200 MeV is natural for a 400 MeV excited hadronic resonance state, once presence of the medium removes superselection constraints.

Another proposed explanation of the K^* , $\Lambda(1520)$ riddle is that there is K^* yield enhancement by regeneration [22]. This $\pi + K \rightarrow K^*$ production mechanism is generally associated with a long lived hadron phase. Factor 5 enhancement over statistical hadronization yield is needed so that given the life span difference, the apparent reduction of $\Lambda(1520)$ by factor 2 is consistent with the observed high K^* yield. We are assuming here that the regeneration of $\Lambda(1520)$ by N, K collisions is not significant. However, a

large K^* yield enhancement contradicts basic principles, in that the heavy K^* would compete with K in the overall bare yield. For this reason, we do not believe that this is a viable explanation.

We conclude that the statistical hadronization is doing reasonably well, the predictions in general agree with experiment in considerable detail, and where strong deviation is observed ($\Lambda(1520)$) a good reason for this is at hand. Resonances test both statistical hadronization, and the nature of the hadronization process [23], and open a path to study in medium modifications of particle hadronic widths.

2.2. Chemical fugacities

The freeze out temperature determines the shape of initially produced particle spectra, and thus it has considerable influence over their yield as well. However, the normalization of the spectra and thus particle yields are more directly controlled by the particle fugacity $\Upsilon_i \equiv e^{\sigma_i/T}$, where σ_i is particle ‘ i ’ chemical potential. Since for each related particle and antiparticle pair we need two chemical potentials, it has become convenient to choose parameters such that we can control the difference, and sum of these separately. For example for nucleons and antinucleons N, \bar{N} the two chemical factors are chosen as:

$$\sigma_N \equiv \mu_b + T \ln \gamma_N, \quad \sigma_{\bar{N}} \equiv -\mu_b + T \ln \gamma_N, \quad (3)$$

$$\Upsilon_N = \gamma_N e^{\mu_b/T}, \quad \Upsilon_{\bar{N}} = \gamma_N e^{-\mu_b/T}. \quad (4)$$

The role of the two factors can be understood considering the first law of thermodynamics:

$$\begin{aligned} dE + P dV - T dS &= \sigma_N dN + \sigma_{\bar{N}} d\bar{N}, \\ &= \mu_b (dN - d\bar{N}) + T \ln \gamma_N (dN + d\bar{N}). \end{aligned} \quad (5)$$

The (baryo)chemical potential μ_b , controls the baryon number, arising from the particle difference. γ_N , the phase space occupancy, regulates the number of nucleon–antinucleon pairs present.

There are many different hadrons, and in principle, we should assign to each a chemical potential and then look for chemical reactions which relate these chemical potentials. However, more direct way to accomplish the same objective consists in characterizing each particle by the valance quark content [25], forming a product of chemical factors, *e.g.*, for $p(uud)$,

$$\Upsilon_{p(uud)} = \gamma_u^2 \gamma_d \lambda_u^2 \lambda_d, \quad \Upsilon_{\bar{p}(\bar{u}\bar{u}\bar{d})} = \gamma_u^2 \gamma_d \lambda_u^{-2} \lambda_d^{-1}.$$

Considering the isospin symmetry of strong interactions aside of the three quark fugacities $\gamma_i, i = u, d, s$, we also introduce the light quark fugacity:

$$\lambda_q^2 = \lambda_u \lambda_d, \quad \lambda_b = \lambda_q^3. \quad (6)$$

To transcribe the fugacities into chemical potentials we recall:

$$\lambda_i = e^{\mu_i/T}, \quad \mu_q = \frac{1}{2}(\mu_u + \mu_d). \quad (7)$$

The relation between quark based chemical potentials and the two principal hadron based chemical potentials of baryon number and hadron strangeness $\mu_i, i = b, S$ is:

$$\mu_b = 3\mu_q, \quad \mu_s = \frac{1}{3}\mu_b - \mu_S, \quad \lambda_s = \frac{\lambda_q}{\lambda_S}. \quad (8)$$

An important (historical) anomaly is the negative S-strangeness in s-hadrons, *e.g.*:

$$\begin{aligned} \Upsilon_\Lambda &= \gamma_u \gamma_d \gamma_s e^{(\mu_u + \mu_d + \mu_s)/T} = \gamma_u \gamma_d \gamma_s e^{(\mu_b - \mu_S)/T}, \\ \Upsilon_{\bar{\Lambda}} &= \gamma_u \gamma_d \gamma_s e^{(-\mu_u - \mu_d - \mu_s)/T} = \gamma_u \gamma_d \gamma_s e^{(-\mu_b + \mu_S)/T}. \end{aligned}$$

There are two types of chemical factors γ_i and μ_i and thus two types of chemical equilibria. These are shown in Table I. The absolute equilibrium is reached when the phase space occupancy approaches unity, $\gamma_i \rightarrow 1$. The distribution of flavor (strangeness) among many hadrons is governed by the relative chemical equilibrium.

TABLE I

Four quarks s, \bar{s}, q, \bar{q} require four chemical parameters; right: \bar{q} name of the associated chemical equilibrium.

γ_i	controls overall abundance of quark ($i = q, s$) pairs	Absolute chemical equilibrium
λ_i	controls difference between quarks and antiquarks ($i = q, s$)	Relative chemical equilibrium

There is considerable difference in the dynamics of these two particle yield equilibration. This can be, *e.g.*, understood considering strangeness in the hadronic gas phase. The two principal chemical processes are seen in Fig. 1. The redistribution of strangeness among (in this example) Λ, π and N, K seen on left in Fig. 1. constitutes approach to the relative chemical equilibrium of these species. The s, \bar{s} pair production process, on right in Fig. 1, is responsible for absolute chemical equilibrium of strangeness. Achievement of the absolute equilibrium, $\gamma \rightarrow 1$, require more rarely occurring truly inelastic collisions with creation of new particle pairs.

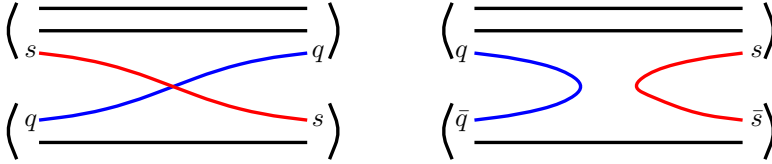


Fig. 1. Typical strangeness exchange (left) and production (right) reactions in the hadronic gas phase.

2.3. Ratios of particle yields

When particles are produced in hadronization, we speak of chemical freeze-out. To obtain the particle yields up to overall normalization the individual Fermi–Dirac and Bose–Einstein phase space integrals are evaluated. In order to arrive at the full yield, one has to be sure to include all the hadronic resonance decays feeding into the yield considered, *e.g.*, the decay $K^* \rightarrow K + \pi$ feeds into K and π yields. This actually constitutes a book keeping challenge in study of particle multiplicities, since decays are contributing at the 50% level to practically all particle yields. Sometimes the decay contribution can be dominant, as is generally the case for the pion yield. For pions in particular, each resonance contributes relatively little in the final count, it is the large number of resonances that contribute which competes with the direct pion yield.

To determine the parameters governing the chemical freeze-out, we analyze particle yields in terms of the chemical parameters and the temperature. Except for direct pions practically always one can use Boltzmann approximation and large reaction volume, and what follows in this subsection assumes that this simple situation applies.

It is often appropriate to study ratios of particle yields as these can be chosen such that certain physical features can be isolated. For example, just the two ratios,

$$R_\Lambda = \frac{\bar{\Lambda} + \bar{\Sigma}^0 + \bar{\Sigma}^* + \dots}{\Lambda + \Sigma^0 + \Sigma^* + \dots} = \frac{\bar{s}\bar{q}\bar{q}}{sqq} = \lambda_s^{-2}\lambda_q^{-4} = e^{2\mu_s/T}e^{-2\mu_b/T}, \quad (9)$$

$$R_\Xi = \frac{\bar{\Xi}^- + \bar{\Xi}^* + \dots}{\Xi^- + \Xi^* + \dots} = \frac{\bar{s}\bar{s}\bar{q}}{ssq} = \lambda_s^{-4}\lambda_q^{-2} = e^{4\mu_s/T}e^{-2\mu_b/T}, \quad (10)$$

lead to a very good estimate of the baryochemical potential and strange chemical potential [26], and thus to predictions of other particle ratios.

The sensitivity to phase space occupancy factors γ_i derives from comparison of hadron yields with differing q, s quark content, *e.g.*:

$$\frac{\Xi^-(dss)}{\Lambda(dds)} \propto \frac{\gamma_d\gamma_s^2}{\gamma_d^2\gamma_s} \frac{g_\Xi\lambda_d\lambda_s^2}{g_\Lambda\lambda_d^2\lambda_s}, \quad \frac{\bar{\Xi}^-(\bar{d}\bar{s}\bar{s})}{\bar{\Lambda}(\bar{d}\bar{d}\bar{s})} \propto \frac{\gamma_d\gamma_s^2}{\gamma_d^2\gamma_s} \frac{g_\Xi\lambda_d^{-1}\lambda_s^{-2}}{g_\Lambda\lambda_d^{-2}\lambda_s^{-1}}. \quad (11)$$

In Eq. (11), each of the ratios also contain chemical potential factors λ_i . These can be eliminated by taking the product of particle ratio with antiparticle ratio, thus

$$\frac{\Xi^-(dss) \bar{\Xi}^-(\bar{u}\bar{s}\bar{s})}{\Lambda(uds) \bar{\Lambda}(\bar{d}\bar{d}\bar{s})} = C_{\Xi\Lambda}^2 \left(\frac{\gamma_s g_{\Xi}}{\gamma_u g_{\Lambda}} \right)^2. \quad (12)$$

The proportionality constant $C_{\Xi\Lambda}^2$ describes the phase space size ratio for the two particles of different mass. It incorporates the contributions from resonance decays, which of course differ from particle to particle.

The method applied in Eq. (12) can be used in several other such double particle ratios. The relevance of this is that we have identified an experimental observable (combination of particle ratios) solely dependent on two parameters of statistical hadronization and chemical freeze-out, the temperature T which controls the phase space factor ratio C and the ratio γ_s/γ_q . Another double ratio of considerable importance is

$$\frac{\Lambda(uds) \bar{\Lambda}(\bar{u}\bar{d}\bar{s})}{p(uud) \bar{p}(\bar{u}\bar{u}\bar{d})} = C_{\Lambda p}^2 \left(\frac{\gamma_s g_{\Lambda}}{\gamma_u g_p} \right)^2. \quad (13)$$

Both ratios Eqs. (12), (13) are independent of chemical potentials, their measurement allows to constrain the value of γ_s/γ_q only as function of T [18].

Double ratio made of mesons in general will be weakly dependent on chemical potentials since some kaons and pions are decay products of baryonic resonances. The leading term is in general originating in direct and resonance mesons, for example:

$$\frac{K^+(u\bar{s}) K^-(\bar{u}s)}{\pi^+(u\bar{d}) \pi^-(\bar{u}d)} = C_{K\pi}^2 \left(\frac{\gamma_s g_K}{\gamma_q g_{\pi}} \right)^2 + \dots. \quad (14)$$

In summary, and for the benefit of our later discussion in Subsection 5.1, we remember that there is no dependence in Eqs. (12), (13) and almost none in Eq. (14) on the baryochemical potential and strange chemical potential. This eliminates dependence of the baryon and strangeness density, and allows to focus on the physics issues unrelated to baryon compression effects.

2.4. Particle phase space density and hadronization

The maximization of microcanonical entropy,

$$S_{F,B} = \int \frac{d^3p d^3x}{(2\pi\hbar)^3} \mp [(1 \mp f_{F,B}) \ln(1 \mp f_{F,B}) - f_{F,B} \ln f_{F,B}], \quad (15)$$

(where indeed minus sign is for fermions and plus sign for bosons) subject to energy and baryon number conservation implies the quantum distributions [24]:

$$\frac{d^6 N_i}{d^3 p d^3 x} = \frac{g_i}{(2\pi)^3} \frac{1}{\Upsilon_i^{-1} e^{E_i/T} \pm 1}, \quad \Upsilon_i^{\text{bosons}} \leq e^{m_i/T}. \quad (16)$$

When the phase space is not densely occupied, ± 1 in the denominator can be neglected and we have the Boltzmann approximation we used in last subsection:

$$\frac{d^6 N_i}{d^3 p d^3 x} = g_i \frac{\Upsilon_i}{(2\pi)^3} e^{-E_i/T}. \quad (17)$$

In Eq. (16), for the Boson distribution, the value of γ_q is limited by the condensation singularity. The maximum value of $\gamma_q^{\text{max}} = e^{m_\pi/(2T)}$ plays a very pivotal role considering that the mass of the pion and hadronization temperature are similar. Large value of $\gamma_q \rightarrow e^{m_\pi/T}$ can be directly noticed in pion spectra in an uptilt in the soft portion of the m_\perp distribution. A similar constraint is also arising from kaon condensation for γ_s but it is much less restrictive:

$$\frac{\gamma_s}{\gamma_q} \left(\frac{\lambda_s}{\lambda_q} \right)^{\pm 1} < e^{(m_K - m_\pi)/T} \simeq 11. \quad (18)$$

In the local restframe the particle yields are proportional to the momentum integrals of the distribution Eq. (16). As example, for pions π , nucleons N and antinucleons \bar{N} we have:

$$N_\pi = CV g_\pi \int_R \frac{d^3 p}{(2\pi)^3} \frac{1}{\gamma_q^{-2} e^{\sqrt{m_\pi^2 + p^2}/T} - 1}, \quad \gamma_q^2 < e^{m_\pi/T}, \quad (19)$$

$$N = CV g_N \int_R \frac{d^3 p}{(2\pi)^3} \frac{1}{1 + \gamma_q^{-3} \lambda_q^{-3} e^{E/T}}, \quad (20)$$

$$\bar{N} = CV g_N \int_R \frac{d^3 p}{(2\pi)^3} \frac{1}{1 + \gamma_q^{-3} \lambda_q^{+3} e^{E/T}}. \quad (21)$$

Naively, we would think that the coefficient is simply the volume V , as it would be the case for a gas of hadrons. However, more generally there is a common additional factor C which is determined by the dynamics of the hadronization process. The region of integration R is determined in terms of the experimental acceptance, keeping in mind that we are here considering the phase space in rest frame of hadronizing QGP, while the experimental

detector is at rest in the laboratory. Both the motion of the collision center of momentum frame with respect to the detector, and the collective flow of QGP have to be allowed for.

Generally a small region of particle rapidity y but nearly all of range of m_{\perp} is accepted in experiments at RHIC. Assuming the yield of particles is practically constant as function of y , it is possible to imagine that the yield arise from a series of fireballs placed at different rapidities. Thus in this limit we can proceed to study hadronization as if we had a full phase space coverage. However, in this case in particular the proportionality constant C can be quite different from unity.

The hadronization of QGP phase is not fully understood. However, numerous experimental indicators show that hadrons are emerging rapidly from a relatively small space-time volume domain. In such a case, hadron formation has to absorb the high entropy content of QGP which originates in broken color bonds. The lightest hadron is pion and most entropy per energy is consumed in hadronization by producing these particles abundantly. We evaluate Eq. (19) to find particle number, and the entropy content follows from Eq. (15):

$$S_{\pi} = \int \frac{d^3p d^3x}{(2\pi\hbar)^3} [(1 + f_{\pi}) \ln(1 + f_{\pi}) - f_{\pi} \ln f_{\pi}] , \quad (22)$$

$$f_{\pi}(E) = \frac{1}{\gamma_q^{-2} e^{E_{\pi}/T} - 1} , \quad E_{\pi} = \sqrt{m_{\pi}^2 + p^2} . \quad (23)$$

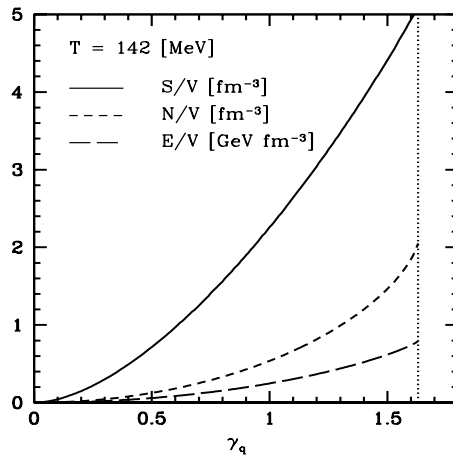


Fig. 2. Entropy density S/V along with particle density N/V and energy density E/V as function of γ_q at $T = 142$ MeV.

As is seen in Fig. 2, the maximum entropy density S/V occurs for an oversaturated pion gas, $\gamma_q \simeq e^{m_\pi/2T} \simeq 1.6$. Here, the entropy density of such a saturated Bose gas is twice as large as that of chemically equilibrated Bose gas. Since aside of pions also many other hadrons are produced, the large value of γ_q is necessary and sufficient to allow for the smooth in μ_b, T, V transformation of a QGP into hadrons. The number of active degrees of freedom in the oversaturated hadron gas with $\gamma_q \rightarrow \gamma_s^{\max}$ and in ‘freezing’ QGP phase is very similar.

3. Strangeness — a popular QGP diagnostic tool

3.1. Motivation for study of strangeness

It is widely agreed that the process of strange particle production in relativistic nuclear collisions offers considerable insight into the structure and dynamics of the dense matter formed in these reactions. The experimental reasons for the interest are practical, as this observable is experimentally accessible. The theoretical interest has been motivated by the recognition that strangeness is a marker of the thermal gluonic degree of freedom of the deconfined phase [27,28]. These result is enhanced abundance of strangeness, and thus production of numerous strange hadrons [29].

In an nutshell the experimental motivation for study of strangeness is:

- There are many strange particles allowing to study different physics questions ($q = u, d$):

$$\phi(s\bar{s}), K(q\bar{s}), \bar{K}(\bar{q}s), \Lambda(qqs), \bar{\Lambda}(\bar{q}\bar{q}\bar{s}), \Xi(qss), \bar{\Xi}(\bar{q}\bar{s}\bar{s}), \Omega(sss), \bar{\Omega}(\bar{s}\bar{s}\bar{s});$$

- Strange hadrons are subject to a self analyzing decay within a few cm from the point of production. As an example, we see the cascading decay of a doubly strange Ξ^- in Fig. 3;

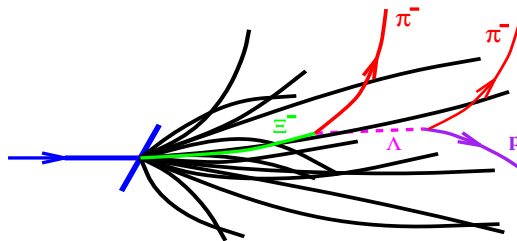


Fig. 3. Ξ^- -decay, dashed line the invisible Λ emerging from the decay kink ending in the decay ‘V’ of the final state charged particles.

- Though some of the strange hadrons are produced quite rarely in p - p reactions, the enhancement we encounter in A - A reactions produces ‘exotic’ strange observables with yields sufficient to reach a relatively high statistical significance.

The theoretical case for study of strangeness has been researched in depth:

- Production of strangeness occurs predominantly in gluon fusion $gg \rightarrow s\bar{s}$. Thus abundant strangeness is linked to presence of thermal gluons from QGP. The quark process [30], $q\bar{q} \rightarrow s\bar{s}$, contributes at level of 10–15% of total rate, the Feynman diagrams for the lowest order process are seen in Fig. 4;

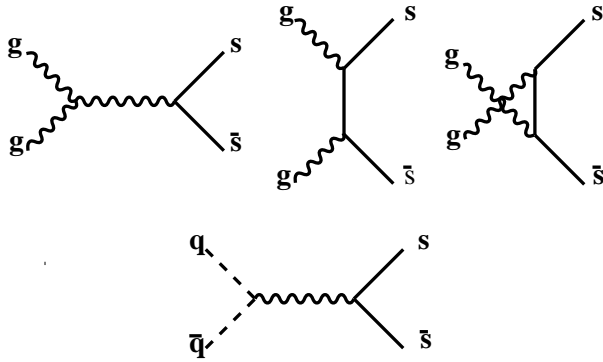


Fig. 4. Lowest order Feynman diagrams for the production of flavor. Top line: gluon fusion and bottom line: quark–antiquark fusion into strange quark pair.

- Coincidence of scales: $m_s \simeq T_c$ implies that the relaxation time required to equilibrate strangeness yield chemically, τ_s , is of the same magnitude as the lifespan of QGP, $\tau_s \simeq \tau_{\text{QGP}}$. In consequence, strangeness acts as a clock for the precise QGP lifespan.
- Due to presence of baryon density, the yield of light antiquarks is suppressed compared to yield of quarks and one thus can encounter $\bar{s} > \bar{q}$. Ensuing recombination production of antibaryons at hadronization of QGP can lead to a relative strange antibaryon enhancement, and at RHIC to (anti)hyperon dominance of (anti)baryons [31].

3.2. Two step hadron formation mechanism in QGP

The establishment of a ready supply of strange quarks occurs in a manner independent of the production of final state hadrons. After some time has passed, QGP drop reaches hadronization condition in its internal pressure

driven expansion. Then, the final state hadrons emerge, as is seen in Fig. 5. Thus strange hadron production occurs in two independent steps following each other in time:

1. $gg \rightarrow s\bar{s}$ predominantly in the early hot QGP;
2. hadronization of pre-formed s , \bar{s} quarks after QGP cools.

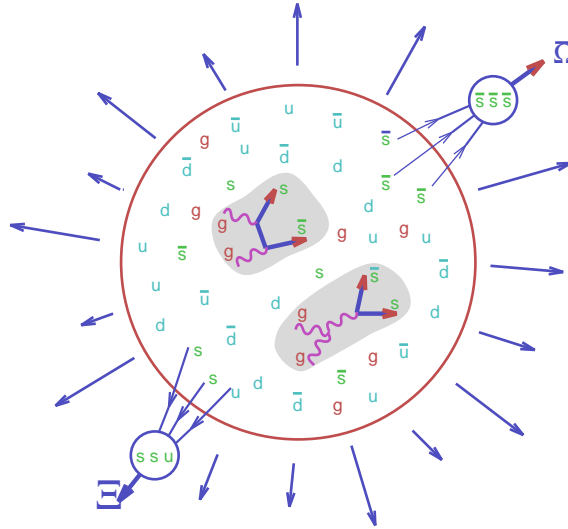


Fig. 5. Illustration of the cross-talk two step mechanism of strange hadron formation from QGP: inserts show gluon fusion into strangeness, followed by QGP recombinant hadronization.

This sequence allows the production of complex rarely produced multi strange (anti)particles, enabled by ‘cross talk’ between s , \bar{s} quarks made in different microscopic reactions. We consider observation of this process to be a specific signature of deconfinement, since it provides evidence for both the activity of thermal gluons, and the mobility of strange quarks. The specific feature of such an enhancement is that the enhanced production of strange antibaryons is increasing with strangeness content.

3.3. Strange hadron enhancement or suppression?

The enhancement of strange hadrons has been studied as function of the number of participating baryons, which are evaluated in terms of ‘wounded nucleons’, that is nucleons which have been involved in an inelastic scattering in the collision. We show, in Fig. 6, the results of NA57 [32, 33], which extend those presented by WA97 collaboration. The yield of strange hadrons

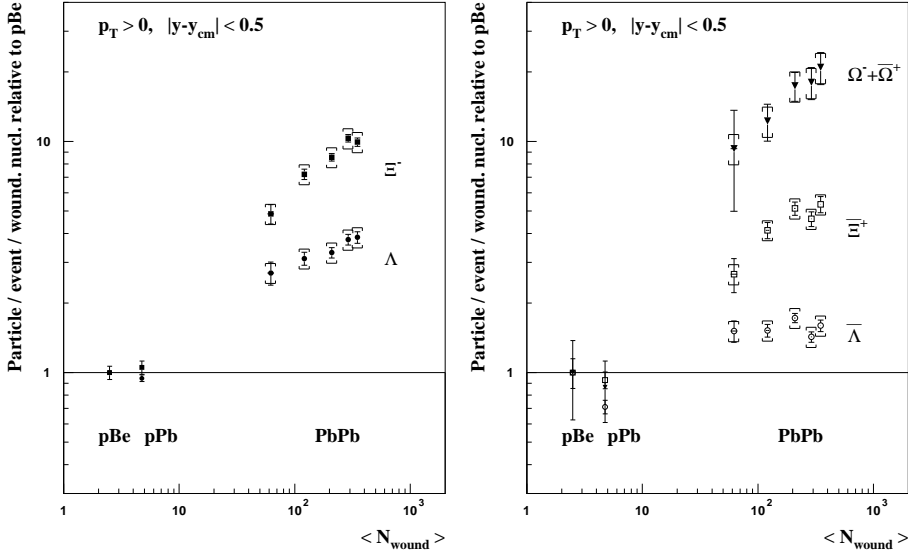


Fig. 6. Specific yield per wounded nucleon of strange baryons Λ , Ξ and antibaryons $\bar{\Lambda}$, $\bar{\Xi}$ and of $\Omega + \bar{\Omega}$ as function of the number of wounded nucleons [33]. The data are obtained in 5 centrality bins which cover the range 50–350 participants. The baseline for the enhancement is the yield observed in the p –Be reactions.

shows the expected increase of enhancement as function of newly made quark content s, \bar{s}, \bar{q} , and as function of the participant number (see for example the result shown in figure 37, in [34]). The enhancement is in Fig. 6 reported with a base for p –Be reactions. It has been recognized long ago that the relatively small number of strange quarks produced in proton induced reaction could require evaluation of statistical yields applying microscopic particle number constraints of relevance in such a limit [35]. Thus statistical equilibrium yields for the p – p reaction systems are suppressed and thus enhancement is seen comparing AA to pp . However, results of NA57 we see in Fig. 6 disagree with the expected behavior of this suppression [36].

Without going into the theoretical details discussed elsewhere [37], the important feature of the micro-canonical yield suppression is that the asymptotic particle yields are relatively quickly attained as is seen in Fig. 7. We see here the enhancement E_i generated by rebasing the small system yields to unity for the strangeness content $i = 1, 2, 3$. The top of the figure shows the resulting enhancement for the p – p reaction system while the bottom estimates the result for p –Be as used by NA57, assuming that the yield of strange quarks pairs $\langle N_s \rangle$ doubles from 0.66 to 1.3. The size dependence is expressed in terms of the canonical yield of strange quarks produced (thus the base enhancement unity is at the value $N^{\text{CE}} = 0.66$ in the top portion of Fig. 7, while it is at $N^{\text{CE}} = 1.3$ in the bottom portion).

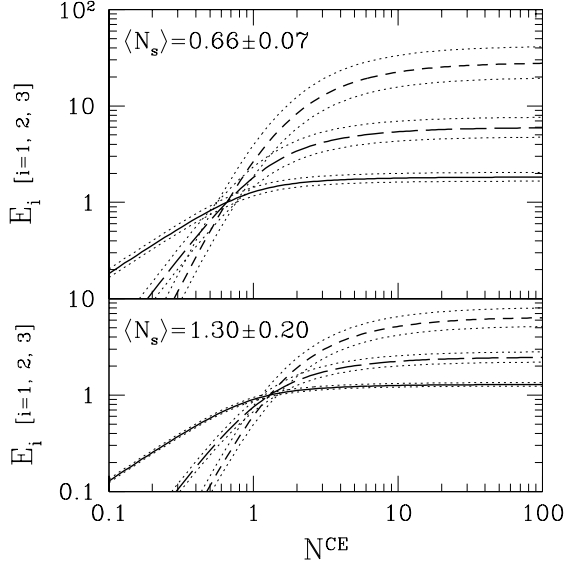


Fig. 7. Enhancement E_i of strangeness $i = 1$ (solid lines), $i = 2$ (long dashed lines) and $i = 3$ (short dashed lines) hadrons as function of the canonical yield of strangeness N^{CE} . The cases for p - p (top panel) and p -Be (bottom panel) reactions are shown.

Looking at the results in Fig. 6, we see that systems with 100–300 baryons are still growing in yield. On the other hand we see in Fig. 7 that the saturated yield of strange hadrons is attained at $N^{\text{CE}} = 5$, which yield is attained for a fireball with 10–30 baryons. This, along with the other issues [37], raised earlier shows that the enhancement effect is indeed not due to a suppression of the base of comparison, but is due to kinetic processes already described, *i.e.*, excess strangeness production in QGP and subsequent hadronization process.

3.4. Sudden hadronization

A fireball is not a piece of deconfined matter sitting still. Given its origin in a collision on two atomic nuclei, it is initially made of highly compressed matter. Thus it subsequently undergoes a rapid collective explosive outflow. Such a collective motion of color charged quarks and gluons contributes an important collective component in the pressure, beyond the rest frame thermal pressure. This can be seen considering the stress portion of the energy-momentum tensor:

$$T^{ij} = P\delta_{ij} + (P + \varepsilon)\frac{v_i v_j}{1 - v^2}. \quad (24)$$

The rate of momentum flow vector $\vec{\mathcal{P}}$ at the surface of the fireball is obtained from the energy-stress tensor T_{kl} :

$$\vec{\mathcal{P}} \equiv \widehat{T} \cdot \vec{n} = P\vec{n} + (P + \varepsilon) \frac{\vec{v}_c \vec{v}_c \cdot \vec{n}}{1 - v_c^2}. \quad (25)$$

The pressure and energy comprise both the particle and the vacuum properties:

$$P = P_p - \mathcal{B} \quad \varepsilon = \varepsilon_p + \mathcal{B}.$$

The condition $\vec{\mathcal{P}} = 0$ reads:

$$\mathcal{B}\vec{n} = P_p\vec{n} + (P_p + \varepsilon_p) \frac{\vec{v}_c \vec{v}_c \cdot \vec{n}}{1 - v_c^2}. \quad (26)$$

Multiplying with \vec{n} , we find:

$$\mathcal{B} = P_p + (P_p + \varepsilon_p) \frac{\kappa v_c^2}{1 - v_c^2}, \quad \kappa = \frac{(\vec{v}_c \cdot \vec{n})^2}{v_c^2}. \quad (27)$$

We note that the hadronization hypersurface, and in particular the angular relation between the collective flow direction vector v_c and surface normal direction, defines the force balance condition seen in Eq. (27).

In order to satisfy the condition Eq. (27), we must have $P_p < \mathcal{B}$: the QGP phase pressure $P = P_p - \mathcal{B}$ must be *negative* at hadronization since it has to compensate the effect of the positive dynamical pressure. When $P \rightarrow 0$ and a nonzero velocity of collective flow remains pointing outward, the surface is torn apart in a rapid filamentation instability. This situation can *only* arise since the quark–gluon matter presses again the collective vacuum which is not subject to collective dynamics [38]. In this aspect the dynamics of QGP expansion reminds us of a gas bubble growth within a liquid (cavitation phenomenon).

The hypothesis that hadronization of the QGP deconfined phase formed in high energy nuclear collision is sudden has a relatively long history. In the 1986 review Koch *et al.* [39] note that strange hadrons will be viable observables of QGP should a long lived hadron requilibration not occur. They offered a study of hadron abundances arising from sudden hadronization of strangeness rich QGP. Once data became available, the first analysis of the experimental hadron abundances is carried out within this approach [26]. The important feature of sudden hadronization, the identity of temperatures of diverse hadrons and in particular of baryons and antibaryons is recognized. Shortly after dynamical models of sudden hadronization begin to emerge [40, 41].

Phase boundary for a system at rest between the hadron gas domain and quark–gluon plasma in the μ_b, T plane, is shown in Fig. 8. The solid

thin line is that for hypothetical point hadrons, while dashed line shows the typical estimate for finite volume hadrons. The effect of the ‘wind’ of flow of QCD matter is also seen in Fig. 8, for a geometry of hadronization with $\kappa = 0.6$.

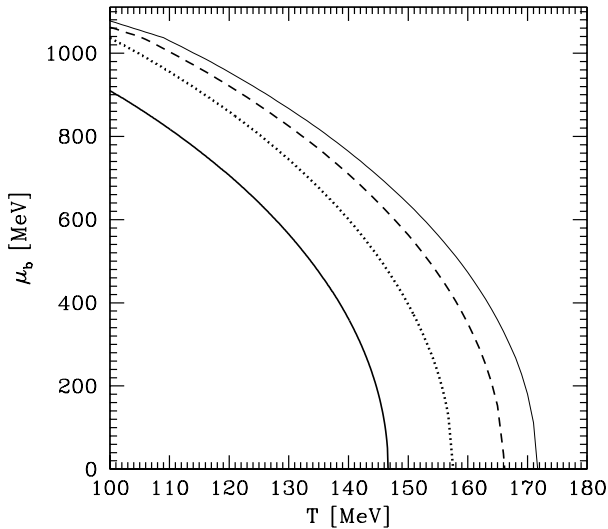


Fig. 8. Hadronization boundary in the μ_b, T plane, QGP–HG transition for point hadrons (solid thin line) and finite volume hadrons (dashed line), are typical estimates of QGP–HG boundary for a system at rest. Dotted line for finite size hadrons includes the effect of the collective flow velocity for $v_c = 0.32$, $\kappa = 0.6$. Thick solid line: breakup with $v = 0.54$, $\kappa = 0.6$ (based on [38]).

As the expansion velocity increases, the magnitude of the color wind effect increases with velocity and is here shown for $v_c = 0.32$ (dotted) and $v_c = 0.54$ (solid lines). With increasing flow velocity the phase boundary moves to lower temperatures. This effect reduces for a given μ_b the magnitude of critical temperature in a significant way.

As collective flow velocity decreases, the hadronization temperature increases. Even though this effect is somewhat compensated by the influence of the increase in μ_b which implies a decrease in T , this ‘normal’ curvature effect seen in each of the lines in Fig. 8 is smaller than the ‘new’ flow effect as we move from line to line in Fig. 8. At RHIC, the largest transverse velocity is reached, and thus largest supercooling achieved. We expect the largest effect from the wind of QGP flow, leading to smallest observed hadronization temperature.

4. Hadronization at SPS and at RHIC

4.1. Method of analysis

We use the statistical hadronization model presented in Section 2 to fit experimental particle yields and to evaluate the hadronization conditions including the specific strangeness, energy and entropy content. Experimental results are now available for several collision energies both at SPS and RHIC. Thus it is possible to study the energy dependence systematically [42]. We will see if there is consistency in the fitted energy dependence both within the energy range of SPS and RHIC, and between these two different energy domains. Specifically, we reevaluate here our comprehensive analysis of RHIC-130 Au–Au collisions [18, 43], carry out a RHIC-200 preliminary analysis and compare with SPS Pb–Pb stationary target reactions at $\sqrt{s_{NN}^{CM}} = 8.75, 12.25, 17.2$ GeV (projectile energy 40, 80, 158A GeV).

For SPS, we use here the CERN-SPS-NA49 4π particle multiplicity results [44, 45], which include π^\pm , K , \bar{K} , Λ , $\bar{\Lambda}$, ϕ at 40, 80, 158A GeV. We also fit (relative) yields of Ξ , $\bar{\Xi}$, Ω , $\bar{\Omega}$ when available. Our current results are found quite near to our earlier work reported for the 158A GeV energy [43], even though our data sample has been limited to (a subset of) NA49 4π -results, while our earlier work was dominated by WA97 central rapidity results. Since we fit only 4π -particle yield, no information about the collective flow velocity is obtained.

Our statistical hadronization program allows for decays of resonances, and for non-equilibrium occupancies of light quarks $\gamma_q \neq 1$ and strange quarks $\gamma_s \neq 1$. In the results, we discuss here, we enforce strangeness conservation. We assume that 50% of weak decays from Ξ to Λ and from Ω to Ξ are inadvertently included in the yields when these had not been corrected for such decays. Particle yields containing this type of contamination from a weak interaction cascade are marked by a subscript ‘c’. We assume that the pions from such weak decays are *not* included in the experimental yields as these pions tracks clearly do not originate in the interaction vertex.

Not all pion producing resonance decays are known, and many have to be guessed given the present status of the particle data tables. We have estimated comparing to expectations based on an exponentially rising mass spectrum that pion yields may be undercounted in the data based statistical hadronization programs [13]. However, one can also argue that pion yield is overcounted: given the sudden nature of the hadron fireball breakup, microscopic reactions cannot exactly follow through to populate the heavy resonances. To estimate the potential for systematic error we study the hadronization with pion yield artificially changed by $\pm 15\%$. We find, not

surprisingly, that there is an anti-correlation to fitted temperature in the range of $\mp 5\%$, respectively, but other statistical parameters and physical properties remain stable.

Some of the particle ratios we consider can be formed from other results already considered. However, each measurement has to be considered as being independent and often the data which theoretically is related by a product of ratios, is in praxis barely consistent. The usual recommended procedure which we follow here is to include all the available *different* particle ratios in the fit, and to include for each measured data point its error in the study of statistical significance. When several experimental results are available for the *same* ratio we fit the average result.

4.2. RHIC analysis

In the study of particle yields at RHIC, we have allowed for both statistical and systematic errors in the experimental data set. We show the results of the fit procedure at RHIC in Table II. The top line gives the reaction energy. The fitted statistical parameters follow, with errors being both statistical and systematic, derived from variation of the pion yield. The equilibrium results for statistical parameters and particle multiplicities agree very well with those presented for the case of chemical equilibrium by the Kraków group [46].

TABLE II

The RHIC chemical freeze-out statistical parameters found for non-equilibrium (left) and semi-equilibrium (right) fits to RHIC results. We show $\sqrt{s_{NN}}$, the temperature T , baryochemical potential μ_b , strange quark chemical potential μ_s , strangeness chemical potential μ_S , the quark occupancy parameters γ_q and γ_s/γ_q , and in the bottom line the statistical significance of the fit. The star (*) indicates that there is an upper limit on the value of $\gamma_q^2 < e^{m_\pi/T}$ (on left), and/or that the value is set (on right).

$\sqrt{s_{NN}}$ [GeV]	200	130	200	130
T [MeV]	143 ± 7	144 ± 3	160 ± 8	160 ± 4
μ_b [MeV]	21.5 ± 31	29.2 ± 4.5	24.5 ± 3	31.4 ± 4.5
μ_s [MeV]	2.5 ± 0.2	3.1 ± 0.2	2.9 ± 0.2	3.6 ± 0.2
μ_S [MeV]	4.7 ± 0.4	6.6 ± 0.4	5.3 ± 0.4	6.9 ± 0.4
γ_q	$1.6 \pm 0.3^*$	$1.6 \pm 0.2^*$	1*	1*
γ_s/γ_q	1.2 ± 0.15	1.3 ± 0.1	1.0 ± 0.1	1.13 ± 0.06
χ^2/dof	2.9/6	15.8/24	4.5/7	32.2/25
P_{true}	90%+	95%+	65%	15%

As the bottom section in Table II shows, the statistical significance is very good for chemical non-equilibrium fit, and also, we note that total χ^2 is half as large as it is for the equilibrium case on the right. Only for a very large number of degrees of freedom one converges toward $\chi^2/\text{dof}=1$ when the experimental errors are correctly evaluated. For a relatively small number of degrees of freedom, as is the case in particular for RHIC-200, we must have χ^2/dof significantly smaller than unity to believe in the physical significance of the result. The bottom line presents an estimate of the probability P_{true} using the values of χ^2 and dof that the fit is an appropriate physics model description. Since the systematic errors are here taken into account, this is an appropriate time to look at this value. Clearly as more data for RHIC-200 becomes available, and errors shrink, this evaluation will change.

TABLE III

ratio	RHIC-130	non-eq fit	χ^2
π^+/p	9.5 ± 1.4	9.07	1.15
π^-/\bar{p}	13.4 ± 0.9	13.15	0.08
\bar{p}/h^-	—	0.0459	—
Λ_c/h^-	0.059 ± 0.004	0.0509	4.11
$\bar{\Lambda}_c/h^-$	0.042 ± 0.004	0.0379	1.04
Ξ_c^-/h^-	0.0079 ± 0.0012	0.00805	0.01
$\bar{\Xi}_c^-/h^-$	0.0066 ± 0.001	0.00645	0.02
Ω/h^-	$(12 \pm 5)10^{-4}$	$13.2 \cdot 10^{-4}$	0.06
$(\bar{\Omega} + \Omega)/h^-$	$(22 \pm 6.5)10^{-4}$	$24.8 \cdot 10^{-4}$	0.19
Λ_c/p	0.90 ± 0.12	0.747	1.63
$\bar{\Lambda}_c/\bar{p}$	0.93 ± 0.19	0.826	0.30
Ξ^-/Λ	0.193 ± 0.03	0.189	0.02
$\bar{\Xi}^-/\bar{\Lambda}$	0.219 ± 0.035	0.207	0.12
Ω/Ξ^-	—	0.164	—
$\bar{\Omega}/\bar{\Xi}^-$	—	0.180	—
$(\bar{\Omega} + \Omega)/(\bar{\Xi} + \Xi)$	0.150 ± 0.04	0.171	0.28
\bar{p}/p	0.71 ± 0.06	0.674	0.36
$\bar{\Lambda}_c/\Lambda_c$	0.71 ± 0.04	0.745	0.78
$\bar{\Xi}/\Xi$	0.83 ± 0.08	0.801	0.13
$\bar{\Omega}/\Omega$	0.95 ± 0.1	0.878	0.51
K^+/π^+	0.17 ± 0.02	0.195	1.59
K^-/π^-	0.15 ± 0.02	0.180	2.28
K^-/K^+	0.87 ± 0.07	0.923	0.57
K^{*0}/K^-	0.26 ± 0.08	0.231	0.13
ϕ/h^-	0.02 ± 0.002	0.0212	0.37
ϕ/K^-	0.15 ± 0.03	0.148	0.00
ϕ/K^{*0}	0.595 ± 0.24	0.639	0.03

One is often interested to see how well the particle yields fit the experiment. For RHIC-130, we obtain the fitted yield ratios of the following 24 results, along with a few (three) results one would wish to also have available (see Table III). It is important that the reader realizes that these ratios can depend significantly on the assumptions made about the cascade of particles that ensues hadronization, and which we cannot fully characterize given lack of experimental data. We have ‘played’ around with branching ratios of high mass resonances and believe that the changes that ensue are all within the errors given for the statistical parameters. However, the individual yields presented below may change, and thus other groups can derive slightly different ratios for same statistical set of parameters.

For RHIC-200 we employ the following 10 relative yields available at this time (see Table IV). We see that the presented non-equilibrium multiplicity fits are good, and the individual contributions to χ^2 are satisfactory.

TABLE IV

ratio	RHIC-200	non-eq fit	χ^2
π^+/p	—	9.86	—
π^-/\bar{p}	12.5 ± 1.7	13.0	0.09
\bar{p}/h^-	—	0.04759	—
Λ_c/h^-	—	0.0441	—
$\bar{\Lambda}_c/h^-$	—	0.0354	—
Ξ_c^-/h^-	—	0.00657	—
$\bar{\Xi}_c^-/h^-$	—	0.00555	—
Ω/h^-	$(8.9 \pm 2)10^{-4}$	$10 \cdot 10^{-4}$	0.31
Λ_c/p	—	0.687	—
$\bar{\Lambda}_c/\bar{p}$	—	0.738	—
Ξ^-/Λ	—	0.175	—
$\bar{\Xi}^-/\bar{\Lambda}$	—	0.187	—
Ω/Ξ^-	—	0.152	—
$\bar{\Omega}/\bar{\Xi}^-$	—	0.162	—
\bar{p}/p	0.74 ± 0.04	0.746	0.02
$\bar{\Lambda}_c/\Lambda_c$	—	0.801	—
$\bar{\Xi}/\Xi$	—	0.844	—
$\bar{\Omega}/\Omega$	1.05 ± 0.2	0.902	0.55
K^+/π^+	—	0.182	—
K^-/π^-	0.156 ± 0.02	0.172	0.63
K^-/K^+	0.95 ± 0.05	0.945	0.01
K^{*0}/K^-	0.205 ± 0.033	0.227	0.44
ϕ/h^-	0.02 ± 0.002	0.0183	0.74
ϕ/K^-	0.118 ± 0.04	0.133	0.14
ϕ/K^{*0}	0.595 ± 0.123	0.585	0.01

The quality of RHIC results presented in Table II confirms that the statistical hadronization mechanism is an appropriate particle production model in presence of the *sudden QGP breakup* which without doubt is seen at RHIC. However, the statistical hadronization approach may be not entirely appropriate at low SPS energies, and all AGS energies. It is possible that kinetic models need to be applied, which allow for a multitude of freeze-out conditions depending on the nature of particle considered. For this reason, when we study this energy domain we will look more closely at the behavior of individual observable (K/π) rather than at the global yields of all particles, the method we are using at RHIC and high SPS energies.

4.3. Phase space occupancy, energy stopping as function of collision energy

The non-equilibrium parameters γ_s, γ_q we find in our fits are shown in Fig. 9 as function of collision energy. In top figure, open squares show the result when we fix $\gamma_q = 1$. We note that in this case the SPS fits yield $\gamma_s \simeq 0.7$. However, we see that $\gamma_q > 1$ is preferred in all cases, with value converging toward the limit $\gamma_q \rightarrow \gamma_q^{\max} = e^{m_\pi/2T}$. This behavior reflects on the need to account for the excess in charged hadron multiplicity. With this large γ_q also γ_s is found to be quite large, in particular so at RHIC. We need to solidify this result since this is indeed the expected signature of the sudden hadronization of deconfined strangeness rich QGP phase.

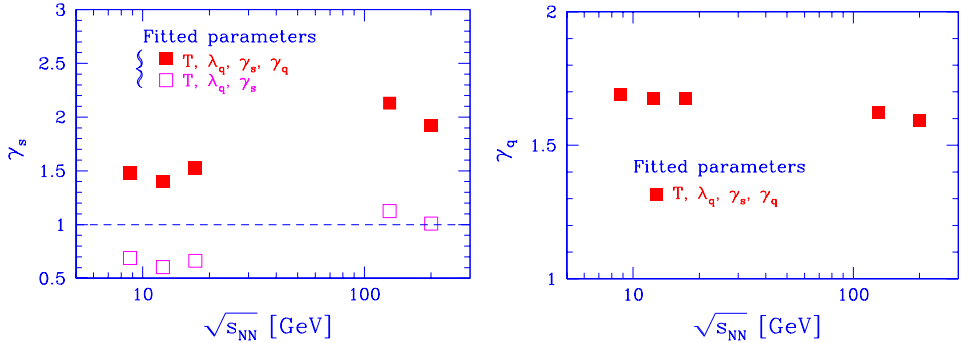


Fig. 9. Fits of, top to bottom γ_s (left) and γ_q (right) chemical non-equilibrium parameters as function of collision energy. Open squares results for $\gamma_q = 1$.

We next address the reaction mechanisms, evaluating the energy stopping. We define it as the ratio of the thermal energy E_{iNN}^{th} found in particles produced and normalized to a nucleon pair, with the collision energy $\sqrt{s_{NN}}$ which is also given per colliding nucleon pair. This study will allow us to consider the energy dependence of other variables as function of the energy

available E_{iNN}^{th} in the fireball, rather than as function of the energy of colliding nuclei $\sqrt{s_{NN}}$, which in its greatest part may not participate in the reaction.

The open triangles Fig. 10 represent energy stopping for the fit assuming full chemical equilibrium. We note that at SPS this leads to the absurd behavior that stopping is increasing with increasing collision energy, reaching 70% at the top energy. This alone proves that the chemical equilibrium approach to statistical hadronization is physically meaningless.

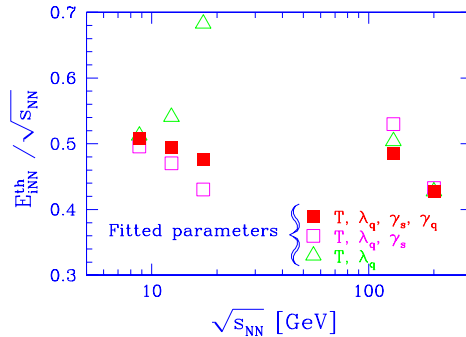


Fig. 10. Fraction of energy stopping at SPS and RHIC: results are shown for 40, 80 and 158 A GeV Pb–Pb fixed target SPS reactions and for 130 and 200 A GeV Au–Au RHIC interactions.

The open squares in Fig. 10 show the stopping found for the case of semi-equilibrium fit, *i.e.*, allowing only strange quarks to be out of chemical equilibrium. The full squares in Fig. 10 apply full chemical non-equilibrium with phase space occupancy shown in Fig. 9. Up to the step-up between SPS and RHIC we see a smooth fall of the stopping with increasing collision energy when chemical non-equilibrium is allowed for. We recall that the statistical hadronization study we have made assumes tacitly that Bjorken rapidity scaling applies exactly. One would hope that the RHIC stopping result will come down when we allow for the non-scaling yields of particles.

4.4. Strangeness and entropy in statistical hadronization

We would like to compare the efficiency of strangeness and entropy production between the two widely different systems considered. We evaluate the number of strange quark pairs produced (strangeness yield) and divide it by the computed thermal fireball baryon number. This eliminates the need for an absolute yield normalization. More generally, a ratio of two extensive computed variables is nearly independent of the dynamics of hadronization.

In Fig. 11, we present strangeness production per baryon. The top Fig. 11 section shows our result as a function of the collision energy. When using

the thermal energy content in the reaction, we arrive at the result with a smoothly rising curve seen in the bottom figure section. As noted in the insert, strangeness yield is rising faster than linearly with fireball energy content.

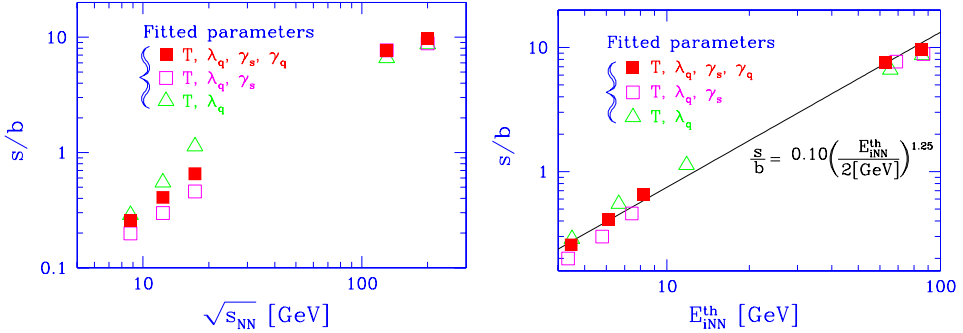


Fig. 11. Strangeness per thermal baryon participant, s/b as function of $\sqrt{s_{NN}}$ (left), and as function of thermal specific energy content E_{iNN}^{th} (right).

We next look at strangeness per entropy, s/S , shown in Fig. 12. There is considerable physical importance of s/S , since both entropy S and strangeness s are produced early on in kinetic processes, are nearly conserved in the hydrodynamical expansion of QGP, and increase only moderately in the hadronization of QGP. Thus the value seen for s/S is reflecting on the kinetic mechanisms operational in early stages of the heavy ion collision. Because there is strangeness mass as energy threshold to overcome, one would expect that as the initial QGP phase becomes hotter with increasing collision energy, the excitation of strangeness grows more rapidly than excitation of entropy.

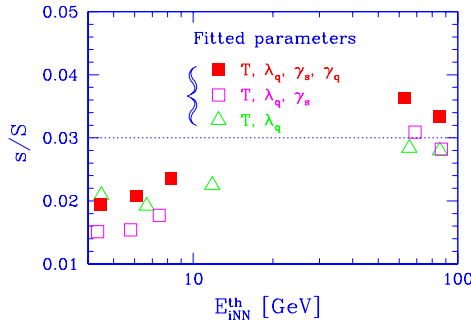


Fig. 12. Strangeness per entropy s/S as function of E_{iNN}^{th} .

We note, in Fig. 12, for the chemical non-equilibrium assumption, a smooth and slow increase of s/S , from 0.02 to 0.025 at SPS. The RHIC-130

point is within the smooth extrapolation of the SPS result. The low value of RHIC-200 result is probably expressing a systematic error related to the absence of multistrange particles in the fit. While entropy is already fully accounted for, only availability of multistrange hadron results will allow to obtain a reliable strangeness yield. However, if this expectation is not fulfilled, it will be very important to obtain experimental results in the energy range between SPS and RHIC, in the domain where the change of the systematic behavior (slope) of s/S as function of energy occurs.

5. Search for an energy threshold

5.1. Kaon to pion ratio

One of the most interesting questions is if there is an energy threshold for the formation of a new state of matter. In our study of strangeness per entropy s/S , in Subsection 4.4, we have seen a possibility that new physics sets in between the SPS and RHIC-130 energy domain. However, a final verdict on this issue depends on further RHIC-200 results.

The NA49 experiment has been exploring the low energy domain at SPS in search for a new physics threshold between AGS and SPS energy range. We refer to the report by Marek Gaździcki for the set of arguments that just at the bottom of SPS energy range something new happens [47]. Perhaps the most important evidence cited by Marek is a peak in the K^+/π^+ ratio, see top section of Fig. 13 [48].

We think that this peak is purely an effect of the dense baryon medium. As the collision energy increases, beginning with low energies, the baryon density increases. However, at some collision energy baryons shoot through and the baryon density begins to drop. Since there is considerable sensitivity to baryon chemical potential and thus baryon density in the K^+/π^+ ratio considered by the NA49 collaboration, we prefer to consider the nearly baryon density independent ratio Eq. (14),

$$\frac{K}{\pi} = \sqrt{\frac{K^+}{\pi^+} \frac{K^-}{\pi^-}}. \quad (28)$$

We present K/π double ratio in the bottom of Fig. 13 as black filled square. At high energy, we show the two RHIC results and at SPS and AGS energies we use the NA49 data set [48, 52]. The open squares are for the charged ratio K^+/π^+ measured in pp reactions, which is offering an upper limit on K/π from pp reactions, also using NA49 data set. We indicate for $\sqrt{s} = 1800$ the $p\bar{p}$ TEVATRON result [51].

Both upper and lower portion of Fig. 13 are drawn on same scale. Comparing the top and bottom in Fig. 13, we see that the peak between AGS

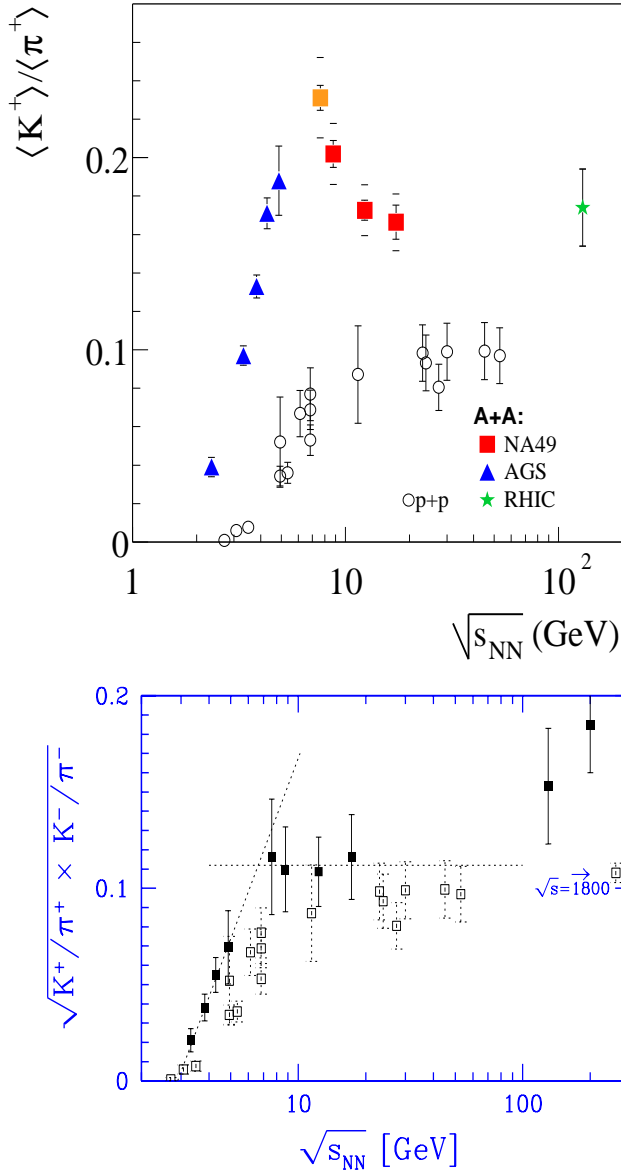


Fig. 13. Top: 4π -ratio of yields of K^+/π^+ for nuclear (filled symbols) and elementary interactions (open symbols); (courtesy of NA49 collaboration [45, 52]). Bottom: the reduced K/π ratio for nuclear (filled) and elementary collisions (open symbols) both as function of collision energy. Figures rescaled to the same magnitude on abscissa and ordinate.

and SPS energy domain has completely disappeared, and that in the SPS energy domain the K/π ratio Eq. (28) is flat. This behavior we already saw in the ratio of strangeness to entropy, bottom of Fig. 11. Moreover, when we look at the inverse slopes of the K^+ m_{\perp} -distributions, Fig. 14, we again see in SPS domain a flat distribution [45].

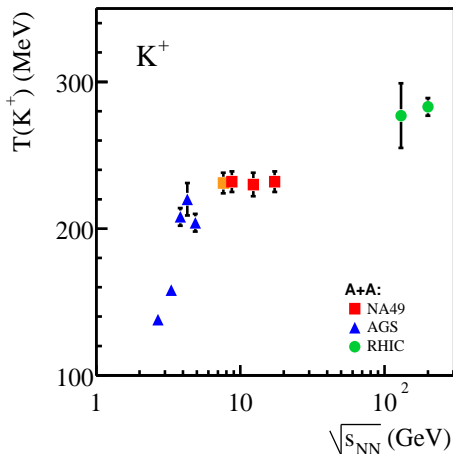


Fig. 14. The inverse slope T of K^+ spectra at AGS (filled triangles) at SPS (filled squares, including a recent 30A GeV NA49 experiment and at RHIC-130 and RHIC-200.

Although the large error bars leave a lot of space for further structure, we do not see any evidence for a ‘peak’ in strangeness production, rather we believe that NA49 has discovered that K^+/π^+ ratio allows to determine where the baryon density peaks as function of collision energy.

As the dashed lines in the bottom portion of Fig. 13 suggest, there is a smooth transition from rising to saturated behavior of K/π ratio. However this behavior mirrors the result we see in the pp reactions, except that it occurs at lower collision energy. *We conclude that if kaon and pion yields are solely used as the measuring stick for new physics, there is clear evidence that new physics is seen at RHIC, where a true deviation from pp , $p\bar{p}$ behavior occurs.*

5.2. A ‘conventional’ K/π excess

The enhancement of K/π ratio at RHIC may be, however, simply result of novel mechanism of pion suppression. We first recall that there is considerable increase in the transverse velocity of matter flow, as is born out, *e.g.*, in the higher inverse slopes of particle spectra at RHIC. We see this effect in Fig. 14 for K^+ .

The kinetic energy of this transverse motion must be taken from the thermal energy of the expanding matter, and ultimately this leads to local cooling and thus a reduction in the number of quarks and gluons. The local entropy density decreases, but the expansion assures that the total entropy still increases. Primarily, gluons are feeding the expansion dynamics, while strangeness being weaker coupled remain least influenced by this dynamics. Model calculations show that there is practically no strangeness reannihilation in transverse expansion at RHIC [53].

The depletion of the non-strange degrees of freedom in the feeding of the expansion assures an increase in the K/π ratio with increase of collision energy. This effect explains why $\gamma_s > \gamma_q$, see Table II. If depletion by transverse expansion dynamics of the non-strange hadrons is the origin of the increase in K/π at RHIC, then this effect would arise gradually as function of collision energy. If, however, new phase of matter is the cause for this increase, we would expect a more ‘edgy’ onset of the increase in the energy domain between SPS and RHIC.

An even greater effect can be expected at future CERN LHC collider. For heavy ions LHC will be a 6000 GeV collider, 30 times the maximum energy at RHIC. The transverse expansion dynamics effects should be much greater at LHC and we expect significantly greater K/π ratio, and thus greater value of γ_s/γ_q . The only limit that we can see for a rise in γ_s/γ_q , which is the factor controlling the rise in K/π , is the condensation limit, Eq. (18):

$$\text{since } \gamma_q^2 \leq e^{\frac{m_\pi}{T}} \text{ and } \gamma_s \gamma_q \leq e^{\frac{m_K}{T}} \text{ we have } \rightarrow \gamma_s/\gamma_q \leq e^{\frac{m_K - m_\pi}{T}}.$$

We have shown the resulting maximal value of K/π in Fig. 15 as a solid line as function of hadronization temperature.

The dashed line in Fig. 15 shows the result when $\gamma_s = \gamma_q = 1$. Depending on what we believe to be a valid hadronization temperature for a fast transversely expanding fireball, the possible enhancement in the K/π ratio will be in the range of a factor 2–3. The arrow indicates whereto the ratio converges for $T \rightarrow \infty$. This limit applies to both solid and dashed lines and critically depends on the high mass resonances which we really do not know very well.

It can be assumed that hadronization at LHC occurs in a temperature domain $T = 160 \pm 20$ MeV. In this case even more interesting than the K/π ratio enhancement would be the associated enhancement anomaly in strange (antibaryon) yields. One would find a strong inversion in the population, with the more strange baryons and antibaryons being more abundant than less strange species.

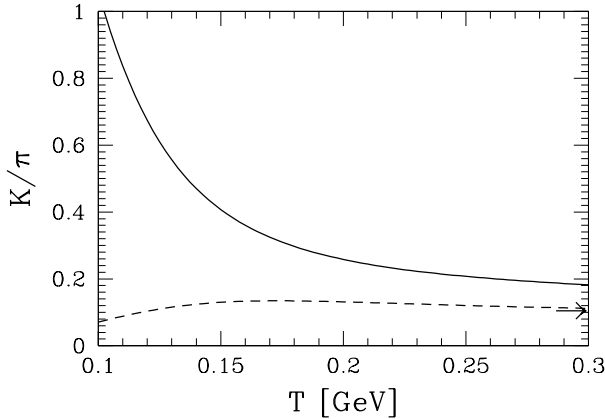


Fig. 15. Kaon to pion ratio K/π (see text) as function of hadronization temperature T for chemical equilibrium (dashed line) and with maximum allowable γ_s and γ_q (solid line).

5.3. Final remarks

We have shown that strangeness at CERN-SPS and BNL-RHIC is a well developed tool allowing to study QGP-hadronization. Our discussion has shown that a systematic study of strange hadrons fingerprints the properties of a new state of matter. We have argued that the deconfinement specific observable is strangeness, and we have explained why we have little doubt that deconfined phase has been formed in relativistic heavy ion collisions.

The situation about deconfinement onset as function of energy is today much less clear than ever before. We argue here (Subsection 5.1) that between AGS and SPS energy range a smooth transition to a saturated K/π yield is seen. This behavior mirrors the behavior of slopes of m_\perp kaon spectra. At SPS, we note a great enhancement of strange antibaryon yields, rising with strangeness content. Analysis of strange hadrons shows that the specific strangeness yield is very high. The strangeness production and hadronization at SPS is consistent with the behavior of the QGP phase.

Somewhere between SPS and RHIC the yield of K/π begins to rise above the elementary reaction result. We saw, in the same energy range, a possible anomaly in the strangeness to entropy ratio s/S , Subsection 4.4. However, we argue in Subsection 5.2 that the K/π ratio rise could be a dynamical effect due to rapid transverse expansion, and we discuss in Subsection 4.4 that the s/S anomaly could be removed by more comprehensive results forthcoming from RHIC-200 run. Thus, at this time, RHIC could harbor some great new discovery, or be a QGP producer with a more powerful transverse expansion and grater energy density. The behavior of particle spectra support this view [54].

The BNL-RHIC experimentalists announced recently the discovery of new physical phenomena, jet quenching, as would be expected in QGP. In February 2000 CERN-SPS experimental groups have combined their experimental results to claim a discovery of new state of matter, which looks like QGP. Aside of strange hadron evidence, several other observables were implicated in the CERN announcement. Discovery of QGP is also claimed in the study of pp reactions [55]. This work evaluates the ideal gas degrees of freedom which number is enhanced as expected in QGP phase.

Though there was not much AGS public relation campaign, we do not see a reason why deconfined state formation did not occur at these low energies. If the criterion of relevance is the heating of nuclear matter to the phase boundary found in lattice gauge calculations, this is achieved at the mid-range of AGS collision energy. However, in this case the new phase of matter is embedded in the center of a opaque hadron shell. Only electromagnetic probes would have allowed to see into the heart of such low energy fireball. A new experimental facility with much more intense beams is needed to perform such experiments.

A student reading this report may find a useful summary of facts about QGP, physics of strangeness, and statistical hadronization. The advanced QGP researcher will find here practical and useful results addressing analysis of the RHIC-130 and RHIC-200 experimental data, and a comparison with SPS results. These results do suggest that through study of strangeness at RHIC we should soon understand better the properties of the hot hadron fireball and its presumably deconfined structure.

Supported by a grant from the U.S. Department of Energy, DE-FG03-95ER40937. Laboratoire de Physique Théorique et Hautes Energies, LPTHE, at University Paris 6 and 7 is supported by CNRS as Unité Mixte de Recherche, UMR7589.

REFERENCES

- [1] P. Carruthers, *Collective Phenomena* **1**, 147 (1973).
- [2] F. Iachello, W.D. Langer, W.D. Lande, *Nucl. Phys.* **A219**, 612 (1974).
- [3] J.C. Collins, M.J. Perry, *Phys. Rev. Lett.* **34**, 1353 (1975).
- [4] J. Rafelski, R. Hagedorn, in *Statistical Mechanics of Quarks and Hadrons*, ed. H. Satz, North Holland, Amsterdam 1981, p. 253.
- [5] R. Hagedorn, *How We Got to QCD Matter from the Hadron Side by Trial and Error*, ed. K. Kajantie, Springer Lecture Notes in Physics, Vol. 221, Springer, Berlin 1985.
- [6] F. Karsch, E. Laermann, A. Peikert, *Phys. Lett.* **B478**, 447 (2000).

- [7] Z. Fodor, S.D. Katz, *Phys. Lett.* **B534**, 87 (2002).
- [8] Z. Fodor, S.D. Katz, *J. High Energy Phys.* **203**, 14 (2002).
- [9] J. Letessier, J. Rafelski, *Phys. Rev.* **C67**, 031902 (2003).
- [10] E. Fermi, *Prog. Theor. Phys.* **5**, 570 (1950).
- [11] E. Fermi, *Phys. Rev.* **92**, 452 (1953).
- [12] J. Letessier, J. Rafelski, *Int. J. Mod. Phys.* **E9**, 107 (2000).
- [13] J. Letessier, J. Rafelski, *Cambridge Monogr. Part. Phys. Nucl. Phys. Cosmol.* **18**, 1 (2002).
- [14] J. Rafelski, J. Letessier, Non-Equilibrium Hadrochemistry in QGP Hadronization, hep-ph/0206145, *AIP Conference Proceedings* **631**, 460 (2002).
- [15] C. Adler *et al.*, *Phys. Rev. Lett.* **89**, 092301 (2002).
- [16] P. Fachini, *J. Phys. G* **28**, 1599 (2002).
- [17] Zhangbu Xu, nuc1-ex/0307014, SQM2003, *J. Phys. G*, in press.
- [18] J. Rafelski, J. Letessier, *Nucl. Phys.* **A715**, 98 (2003).
- [19] C. Markert, *J. Phys. G* **28**, 1753 (2002) and in proceedings of the 19th Winter Workshop on Nuclear Dynamics, Breckenridge, 2003.
- [20] L. Gaudichet, for the STAR Collaboration, nuc1-ex/0307013, SQM2003, *J. Phys. G* in press.
- [21] J. Rafelski, J. Letessier, G. Torrieri, *Phys. Rev.* **C64**, 054907 (2001); Erratum *Phys. Rev.* **C65**, 069902 (2002).
- [22] M. Bleicher, J. Aichelin, *Phys. Lett.* **B530**, 81 (2002).
- [23] G. Torrieri, J. Rafelski, *J. Phys. G* **28**, 1911 (2002).
- [24] J. Letessier, J. Rafelski, A. Tounsi, *Phys. Rev.* **C50**, 406 (1994).
- [25] P. Koch, J. Rafelski, W. Greiner, *Phys. Lett.* **B123**, 151 (1983).
- [26] J. Rafelski, *Phys. Lett.* **B262**, 333 (1991).
- [27] J. Rafelski, B. Müller, *Phys. Rev. Lett* **48**, 1066 (1982); **56**, 2334E (1986).
- [28] J. Rafelski, *Phys. Rep.* **88**, 331 (1982).
- [29] J. Rafelski, Extreme states of nuclear matter. p.282 in *Future Relativistic Heavy Ion Experiments*, Eds. R. Bock, R. Stock, , GSI Report 1981-6 and *Nucl. Phys.* **A374**, 489c (1982).
- [30] T. Biró, J. Zimányi, *Phys. Lett.* **B113**, 6 (1982).
- [31] J. Rafelski, J. Letessier, *Phys. Lett.* **B469**, 12 (1999).
- [32] F. Antinori *et al.*, *Nucl. Phys.* **A698**, 118 (2002).
- [33] V. Manzari *et al.* NA57 Collaboration, *Nucl. Phys.* **A715**, 140 (2003).
- [34] J. Rafelski, J. Letessier, A. Tounsi, *Acta Phys. Pol. B* **27**, 1037 (1996).
- [35] J. Rafelski, M. Danos, *Phys. Lett.* **B97**, 279 (1980).
- [36] S. Hamieh, K. Redlich, A. Tounsi, *Phys. Lett.* **B486**, 61 (2000).
- [37] J. Rafelski, J. Letessier, *J. Phys. G* **28**, 1819 (2002).
- [38] J. Rafelski, J. Letessier, *Phys. Rev. Lett.* **85**, 4695 (2000).

- [39] P. Koch, B. Muller, J. Rafelski, *Phys. Rep.* **142**, 167 (1986).
- [40] T. Csörgő, L.P. Csernai, *Phys. Lett.* **B333**, 494 (1994).
- [41] L.P. Csernai, I.N. Mishustin, *Phys. Rev. Lett.* **74**, 5005 (1995).
- [42] J. Rafelski, J. Letessier, [hep-ph/0305284](#), *J. Phys. G*, in press.
- [43] J. Rafelski, J. Letessier, *Nucl. Phys.* **A702**, 304 (2002).
- [44] V. Friese, [nucl-ex/0305017](#), *J. Phys. G*, in press.
- [45] M. Gaździcki, [hep-ph/0305176](#), *J. Phys. G*, in press, and private communication.
- [46] A. Baran, W. Broniowski, W. Florkowski [nucl-th/0305075](#).
- [47] M. Gaździcki, *Acta Phys. Pol. B* **34**, 5771 (2003).
- [48] S.V. Afanasiev *et al.*, NA49 Collaboration, *Phys. Rev.* **C66**, 054902 (2002).
- [49] C. Adler, *et al.*, STAR Collaboration, [nucl-ex/0206008](#).
- [50] D. Ouerdane, *et al.*, BRAHMS Collaboration, *Nucl. Phys.* **A715**, 478 (2003).
- [51] T. Alexopoulos *et al.*, FNAL E735 Collaboration, *Phys. Rev.* **D48**, 984 (1993).
- [52] M. vanLeeuwen, Compilation of NA49 Results as Function of Collision Energy, private communication (2003).
- [53] J. Rafelski, J. Letessier, *Phys. Lett.* **B469**, 12 (1999).
- [54] W. Broniowski, W. Florkowski *Acta Phys. Pol. B* **33**, 1935 (2002).
- [55] T. Alexopoulos *et al.*, *Phys. Lett.* **B528**, 43 (2002).